

Title:

Age-maintained human neurons demonstrate a developmental loss of intrinsic neurite growth ability

Bo P. Lear^{1†}, Elizabeth A.N. Thompson^{1†}, Kendra Rodriguez¹, Zachary P. Arndt¹, Saniya
5 Khullar³, Payton C. Klosa¹, Ryan J. Lu⁴, Christopher S. Morrow¹, Ryan Risgaard¹, Ella R.
Peterson¹, Brian B. Teefy⁴, Anita Bhattacharyya², Andre M.M. Sousa¹, Daifeng Wang³, Bérénice
A. Benayoun⁴, Darcie L. Moore^{1*}

Affiliations:

¹ *Department of Neuroscience, University of Wisconsin-Madison, Madison, WI*

10 ² *Department of Cellular and Regenerative Biology, University of Wisconsin-Madison, Madison, WI*

³ *Department of Biostatistics and Medical Informatics, Department of Computer Science, University of Wisconsin-Madison, Madison, WI*

⁴ *Leonard Davis School of Gerontology, University of Southern California, Los Angeles, CA*

15 † denotes equal contributions

*Corresponding author, Darcie L. Moore. Email: darcie.moore@wisc.edu

Abstract: Injury to adult mammalian central nervous system (CNS) axons results in limited
20 regeneration. Rodent studies have revealed a developmental switch in CNS axon regenerative
ability, yet whether this is conserved in humans is unknown. Using human fibroblasts from 8
gestational-weeks to 72 years-old, we performed direct reprogramming to transdifferentiate
fibroblasts into induced neurons (Fib-iNs), avoiding pluripotency which restores cells to an
embryonic state. We found that early gestational Fib-iNs grew longer neurites than all other ages,
25 mirroring the developmental switch in regenerative ability in rodents. RNA-sequencing and
screening revealed ARID1A as a developmentally-regulated modifier of neurite growth in human
neurons. These data suggest that age-specific epigenetic changes may drive the intrinsic loss of
neurite growth ability in human CNS neurons during development.

30 **One-Sentence Summary:** Directly-reprogrammed human neurons demonstrate a developmental
decrease in neurite growth ability.

Main text:

Human spinal cord injury (SCI) leads to life-long disability with high medical, psychological, and social costs (1). This injury damages long axonal projections originating from neurons in the brain, which extend through the spinal cord to communicate with the periphery. These central nervous system (CNS) axons fail to regenerate due to both inhibitory proteins in the injured environment, and by a lack of intrinsic axon growth ability in the neurons themselves (2). Interestingly, rodent studies have revealed a link between age and axon growth and regeneration, such that embryonic CNS neurons can extend long axons, while postnatal and adult CNS neurons cannot (3-7). Further, many developmentally-regulated genes, when modulated, can drive axon growth (3, 8-13). However, it is not known whether human neurons also have a developmental switch in CNS axon regenerative ability.

Here, we use an *in vitro*, age-retained, human neuronal model system to identify novel, developmentally-regulated, intrinsic factors which regulate neurite growth. To maintain the age of the originating fibroblasts, we utilized a validated direct reprogramming protocol which transdifferentiates human fibroblasts of different ages directly into induced neurons (Fib-iNs), avoiding pluripotency, which restores cells to an embryonic age (14, 15). In adult cells, the use of direct reprogramming maintains the age of the original cell, and has been shown in many different studies to reveal age-associated disease phenotypes (14-20), however whether prenatal age is similarly maintained with direct reprogramming is not clear. Additionally, direct reprogramming produces neurons which are environmentally naïve, allowing us to determine the role of age on the intrinsic neurite growth ability of human neurons.

Thus, to address these questions, we transdifferentiated human neurons from 11 fibroblast lines ranging from 8 gestational-weeks (GW) through 72 years-old (YO; Table 1) by overexpressing the transcription factors achaete-scute family bHLH transcription factor 1 (ASCL1) and neurogenin 2 (NEUROG2), and culturing cells in the presence of small molecules for 4 weeks (Fig. 1A-B, S1A-B) (14, 15). To first determine the types of neurons being made and the maintenance of age in Fib-iNs at the transcriptional level, we collected all ages of Fib-iNs for RNA-sequencing (RNA-seq). To obtain a pure neuronal population, we transduced Fib-iNs with a lentivirus expressing mScarlet from a hSynapsin promoter and used fluorescence activated cell sorting (FACS) to collect mScarlet⁺ neurons (Fig. S1C-D) to perform low cell number RNA-seq on all ages of Fib-iNs

(Table 1). Samples were corrected for the 5 first genotype principal components (PCs), as determined from RNA-seq data (Fig. S1E), and examined for separation using multi-dimensional scaling (MDS), demonstrating that age-specific replicates clustered similarly (Fig. 1C, S1F).

5 To confirm the neuron subtype specificity in all samples, we immunostained Fib-iNs for beta-III tubulin (TUBB3) together with either vesicular glutamate transporter 1 (VGLUT1; excitatory neurons) or gamma-aminobutyric acid (GABA; inhibitory neurons), and found that the neurons produced were 70.3% +/- 6.7% VGLUT1+ and 16.5% +/-2.4% GABA+, similar to previously published reports (14, 15) (Fig. S1G-H), demonstrating that the neurons are primarily
10 glutamatergic. To gain more detailed knowledge about the type of neurons being produced, we compared our RNA-seq data to the Allen Brain Map single cell RNA-seq data from adult human cortex (21, 22). We again confirmed that all ages of Fib-iNs made excitatory neurons, and the same neuron identity was conserved across the 11 lines (Fig. 1D, Table 1). Specifically, the Fib-iN transcriptional profiles were most similar to excitatory cortical neurons, with the topmost hit being
15 excitatory neurons from layer 6, with FEZ family zinc finger 2 (*FEZF2*) and Tubulin Folding Cofactor C (*TBCC*) as their primary subclass markers and cluster-specific markers, respectively (Fig. 1D). This expression signature was most similar to cells from the primary visual cortex (V1C), middle temporal gyrus (MTG), and cingulate gyrus (CgG). We also identified strong similarities between Fib-iNs to cells from layers 3 and 5 (identifiers: *THEMIS* (subclass), *ELOF1*
20 (cluster-specific) or *UBE2F* (cluster-specific)), whose expression signature was most similar to neurons in the M1 lower limb region of primary motor cortex and M1 upper limb region of primary motor cortex (Fig. 1D). Thus, these analyses confirm that human Fib-iNs are not only excitatory, but resemble human cortical neurons expressing *FEZF2*, a gene required for corticospinal motor neuron identity in rodents (23-25).

25 Use of this model system not only delivers the benefit of producing human neurons, but direct reprogramming also maintains the cellular age of the original cell by bypassing pluripotency during the transdifferentiation (14, 15, 26). This protocol has primarily been used to produce adult neurons from adult fibroblasts for aging studies (27), however there is limited knowledge of the
30 ability to maintain prenatal age during direct reprogramming. To confirm general maintenance of cellular age in the Fib-iNs produced from our fibroblast lines of gestational through adult ages, we first immunostained fibroblasts and Fib-iNs for the nuclear envelope marker LaminB1, a protein

whose levels decrease with aging (16, 28-31). We found a significant decrease in Lamin B1 with increasing age in both fibroblasts and Fib-iNs, confirming maintenance of cellular age with direct reprogramming in our fibroblast lines (Fig. S1I-J). To confirm maintenance of prenatal ages in Fib-iNs, we used the PsychENCODE region-specific, bulk tissue, RNA-seq data of prenatal and postnatal human brain to compare to gestational age Fib-iNs (8GW, 12GW, 20GW#1, 20GW#2, and Neonatal) (32). First, we compared genes significantly up- or downregulated with age in Fib-iNs to genes up- or downregulated in human V1C or M1C, and found genes up- and downregulated in V1C were significantly similar to those in Fib-iNs (Fig. 1E). Further, comparison of genes that were similarly regulated between the two areas (M1C and V1C) to our Fib-iNs revealed a significant similarity between the human tissue data and purified prenatal Fib-iNs (Fig. 1E). Second, to further confirm the maintenance of prenatal ages using this direct reprogramming approach, we trained a machine-learning model using bulk gene expression studies from dissected human M1C and V1C, ages 10GW to 24GW (32), to predict developmental age based on gene expression patterns. Using this model we were able to predict the age of each of our Fib-iN samples from 8GW to neonate, and found, despite comparing purified cultured excitatory neurons (Fib-iNs) to bulk tissue made up of many cell types (PsychENCODE) (32), 8GW to neonatal directly reprogrammed Fib-iNs had increasing predicted age, though with a slight upwards shift of predicted age in the Fib-iNs (Fig. 1F).

Recent studies on gene expression changes during human brain development revealed that the largest change in gene expression occurs during the late-fetal transition, a period beginning around 21GW (32-34). The genes whose expression increases during this late-fetal transition exhibited increased expression levels in postnatal to aged Fib-iNs (Neo-72YO, $p=0.011$), whereas those genes whose expression decreases during the late-fetal transition demonstrated decreased expression in early fetal Fib-iNs (8GW-12GW, $p=0.006$; Fig. 1G). Importantly, these data taken together suggest that prenatal age can be maintained with direct reprogramming, and that gestational Fib-iNs may be used to study neuronal function associated with intrinsic changes occurring during development.

Use of direct reprogramming also maintained transcriptional age in adult Fib-iNs. We found that adult Fib-iNs demonstrated changes in gene expression associated with adult aging, as expected, with 2,431 genes significantly changed ($FDR<5\%$; Fig. 1H). Additionally, we found an increase

in transposable element (TE) expression with age (Fig. S1K), confirming previous reports that TEs levels increase with age (35). Thus, our RNA-seq results support maintenance of age in Fib-iNs at all ages, both during gestation and aging.

5 Rodent CNS neurons undergo a developmental loss of axon growth ability around the time of birth (3, 4, 7, 11, 36, 37). Thus, using this validated human, age-specific model system, we asked if there were differences in intrinsic neurite growth ability among the 11 ages of Fib-iNs (TUBB3+/GABA-/VIM-; Fig. S2A-B). Neurons were dissociated after 4 weeks of transdifferentiation and sorted onto a gelatin substrate to remove remaining fibroblasts and enrich
10 for neurons (Fib-iNs), before plating at low density (100 cells/mm²) on a laminin-coated substrate (Fig. S2C) for 2 days in an axon supportive media (ASM; S2D-H). Interestingly, we found that 8GW and 12GW human neurons grew the longest neurites of all the ages. By 20GW and older, neurons grew only short neurites, demonstrating a developmental decline in neurite growth ability in human neurons (Fig. 2A-B). Interestingly, when comparing neurodevelopmental benchmarks
15 between mouse and human, mouse birth (E21/P0) is equivalent to approximately human 21GW (38), the timing of the late-fetal transition (33), suggesting the conservation of a developmental loss of intrinsic neurite growth ability in our environmentally naïve human neurons (Fig. S2I). Previously, it has been suggested that during neurodevelopment there is a transcriptional shift from elongation to synaptogenesis and branching which limits axon growth ability in rodents postnatally
20 (39, 40). Thus, we measured neurite branching in all ages of Fib-iNs and found that total branching was increased in adult Fib-iNs (Fig. 2C), but this change did not coincide specifically with the time when intrinsic neurite growth ability decreased, nor was there a relationship between the number of branches on the longest neurite and Fib-iN age (Fig. S2J). Thus, we found that human Fib-iNs demonstrate a developmental loss of intrinsic neurite growth ability even in an *in vitro*,
25 environmentally naïve system (Fig. 2A-B).

To confirm that this neurite outgrowth phenotype was specific to the age of the Fib-iNs, we took
5 of the human fibroblast lines (Table 1), and reprogrammed them to iPSCs (Fig. 1A), thus resetting cellular age (Fig. S2K-L) as has been previously shown by others (14-16, 41). We directly
30 reprogrammed these iPSCs to iNs (14) (iPSC-iNs; Fig. 1A, S2M-N), and found there was no longer any difference in the intrinsic neurite growth ability (Fig. 2D-E) of neurons between ages,

demonstrating that the developmental decline in neurite growth ability in Fib-iNs is specific to the preservation of age.

Developmentally-regulated genes identified in rodents have been targeted to reveal age-dependent drivers of CNS axon growth and regeneration (3, 11, 13, 42-44). Thus, we asked which genes were significantly changed between “long-growing” Fib-iNs (8-12GW) versus “short-growing” Fib-iNs (Neo-72YO; Fig. 3A). Due to the neurite growth variability between the 20GW biological replicates and the variability in their “predicted” ages (Fig. 1G, 2B), we grouped both 20GW samples into a “variable condition,” and did not include them in this direct comparison. We identified 3,465 differentially expressed genes (DEGs) between long-growing and short-growing human Fib-iNs at FDR<1% (Fig. 3A, S3A, Table 2), indicating large transcriptional differences in the neurons with different growth phenotypes. Interestingly, using Gene Ontology enrichment analysis, we found enrichments for terms such as translational initiation, ribosomes, and cytoskeleton in long-growing Fib-iNs, whereas tissue-specific immune responses were enriched in short-growing Fib-iNs (Fig. S3A). We next asked how transcripts enriched in long-growing and short-growing Fib-iNs compare to known axon growth and regeneration datasets in rodent studies. Using gene sets from developmentally-regulated rodent CNS neuron studies, we compared the similarity of the transcriptional regulation of these genes to long- and short-growing Fib-iNs, revealing that human Fib-iNs behaved similarly to multiple developmentally-regulated gene sets in rodent retinal ganglion cells, cortical, and callosal neurons (Fig. 3B). However, a similar analysis using rodent axon regeneration datasets revealed less conservation (Fig. 3C). Finally, we curated a list of genes identified in other species to be activators or inhibitors of axon growth and regeneration (though not all developmentally-regulated) and assessed their expression levels across age in Fib-iNs (33, 42, 43, 45-49). Interestingly, we found only a subset of these genes tended to be differentially regulated with age in human Fib-iNs (Fig. S3B). These comparisons suggest that there are largely conserved developmental programs between species (Fig. 3B, S3B), however, regeneration programs have less agreement between rodent neurons and Fib-iNs (Fig. 3C, S3B). It is unclear whether this is due to the lack of orthologs between species for comparison, aspects of the Fib-iN protocol itself, or differences between humans and rodents.

We next used a Weighted Gene Co-expression Network Analysis (WGCNA) to identify modules of genes that behaved similarly, correlated them to phenotypes (long-growing versus short-

growing), and identified significant modules (50, 51). Out of the 216 co-expression modules generated, 62 were significantly correlated with a neurite growth phenotype in our Fib-iNs (Fig. 3D, S3C, Table 3-4). We used the top 6 modules with $R \geq 0.89$ (2 enriched in short growing, and 4 enriched in long growing) and analyzed the genes within each of these modules further (Fig. 3D, Table 4; <https://adsnpheno.shinyapps.io/axonGrowthProject/>). In concordance with our phenotypic characterization, long-growing modules enriched for Metascape (52) terms associated with axon development and many cytoskeleton reorganizing pathways, suggesting the reorganization of the cellular cytoskeleton structure may be necessary for promoting neurite elongation (Fig. 3E). Short-growing modules enriched for terms associated with receptor signaling and energy generation pathways suggesting that short-growing Fib-iNs may spend more energy responding to the environment (Fig. S3D).

To test the hypothesis that developmentally-regulated genes in human neurons could be candidates for modulating axon growth, we selected a short list of genes to screen for their ability to modify neurite outgrowth in Fib-iNs (Table 5). Using the genes in the selected 6 modules and taking into account the combination of the Pearson correlation score, the fold-change in DEGs from the Fib-iN RNA-seq, and whether the genes were also correctly developmentally-regulated in human brain (32), we chose 50 genes to attempt to knockdown (KD) or overexpress (OE) using lentivirus in the appropriate age of Fib-iNs (Fig. 3F-G, S3E). Of the 50 genes tested, 19 genes successfully transduced in our primary screen, and of those 19, 5 genes (26%) significantly modulated neurite growth in the correct direction in either the long-growing or short-growing Fib-iNs, as determined by z-scores (Fig. 3H). In a secondary screen, modulation of 3 of these genes reproducibly significantly modulated neurite growth in the direction predicted from their developmental regulation, including leucine rich repeat kinase 2 (*LRRK2*; coral module), mir9_3p (*MIR9_3HG* was enriched in coral module and mir9_3p regulated many genes in the dark green module), and AT-rich interaction domain 1A (*ARID1A*; darkolivegreen1 module; Fig. 3I-J). *LRRK2* is the most commonly mutated gene in familial Parkinson's Disease (53, 54). Previous studies have found that *LRKK2* OE leads to shortening of neurites, and *LRKK2* knockout leads to increased neurite outgrowth (54), similarly confirmed in our results showing that its KD in adult Fib-iNs (36YO) leads to increased neurite outgrowth (Fig. 3I-J). MicroRNA-9 (miRNA-9) is one of the most abundant miRNAs in the brain and has been shown to decrease axon growth in E17 rodent neurons and play critical roles in dendritic development, synaptic transmission, and axon branching (55-

57). We confirmed a similar role for mir9_3p in human Fib-iNs, where it is upregulated in short-growing neurons, and its overexpression in 8GW neurons leads to reduced neurite growth (Fig. 3I-J). Thus, these data validate the use of developmentally-regulated genes in humans to identify regulators of neurite growth.

5

ARID1A, also known as Brahma-related associated factor 250a (BAF250a), is a DNA-binding subunit of the canonical mammalian SWI/SNF complex, otherwise known as the canonical BAF complex, which preferentially interacts with enhancers. This ATP-dependent chromatin remodeling complex generally functions as an activator of transcription, with critical roles in regulating chromatin changes during development and in cancer (58). Loss-of-function mutations in *ARID1A* can lead to Coffin-Siris Syndrome, a neurodevelopmental disorder with symptoms such as intellectual disability, growth impairment, hypotonia, and structural CNS abnormalities (59), but *ARID1A* is most studied for its role in cancer (60). Interestingly, both loss- or gain-of-function mutations in *ARID1A* can lead to a wide-range of cancers depending on cellular context, and affects pathways including the WNT, P21, PI3K/AKT, YAP/TAZ, IL-6/STAT3, and IFN pathways (60). In the human brain, *ARID1A* mRNA levels decrease during human cortical development (Fig. 4A) (32). To determine if ARID1A protein levels were similarly regulated in human development *in vivo*, we assessed the expression of ARID1A and BCL11B, a marker of deep cortical layers, in 16GW, 21GW, and 42YO human cortices. At 16GW, ARID1A protein is present in most cells of the cortical plate. By 21GW, ARID1A expression becomes more spatially restricted within the cortical plate and is enriched in a subset of BCL11B⁺ neurons. In the adult brain, ARID1A protein levels are dramatically downregulated in the cortex and are lowly expressed across all layers of the cortex (Fig. 4B). These results confirm both published RNA-seq results from human cortical development (Fig. 4A; (32)), and our Fib-iN RNA-seq results (Fig. 4C), demonstrating ARID1A is downregulated across development and aging.

25

Since we found that *ARID1A* KD in long-growing Fib-iNs decreases neurite outgrowth in our screen (Fig. 3I-J, S4A-B), we asked if increasing ARID1A protein levels would be sufficient to increase neurite outgrowth in short-growing Fib-iNs. As ARID1A is a large 250kD protein, we selected CRISPR activation (CRISPRa) to activate its expression in 36YO neurons (short-growing), where a guide RNA (gRNA) localizes an enzymatically dead CRISPR/Cas9 and three transcriptional activators (VP64, HSF1, p65) to the *ARID1A* promoter (OriGene; Fig. S4C). Fib-

30

iNs were transduced with two viruses: one containing a transcriptional enhancer with no reporter, and another containing the gRNA, deadCas9, and GFP (Fig. S4C). We found that GFP+ Fib-iNs transduced with gRNAs targeting *ARID1A* had increased levels of ARID1A protein as compared to the non-targeting gRNA (Fig. 4D-E). Further, we found increased ARID1A protein led to an increase in neurite outgrowth of 36YO Fib-iNs (Fig. 4D, 4F). Thus, taken together, these results demonstrate that modulation of ARID1A protein levels can drive changes in human neurite growth.

As part of the BAF complex, ARID1A primarily targets enhancers thus increasing accessibility for transcription factor binding (61, 62). H3K27acetylation (H3K27ac) is a common epigenetic modification associated with the ARID1A-containing BAF complex (63-66). Rodent dorsal root ganglion neurons have increased global H3K27ac levels following enriched environment conditions which increased axon regeneration, connecting H3K27ac histone modifications with axon growth potential (67-69). KD or loss of ARID1A leads to decreased H3K27ac, resulting in changes in the chromatin architecture (61, 63, 65, 66, 70). Thus, we measured the levels of H3K27ac in 8GW Fib-iNs treated with scrambled or *ARID1A*-targeting shRNA. We found reduced levels of H3K27ac with *ARID1A* KD compared to a scrambled control (Fig. 4G). Further, immunostaining of Fib-iNs across developmental ages revealed 8GW as having the highest H3K27ac signal, with a decrease during development and aging (Fig. 4H). These data suggest ARID1A, a developmentally-regulated protein in human neurons, may promote neurite growth at the chromatin level by increasing levels of H3K27ac, thus controlling transcription of downstream targets.

To identify how modifications in ARID1A affect downstream genes and drive changes in neurite outgrowth in Fib-iNs, we performed RNAseq on 8GW Fib-iNs transduced with *ARID1A* shRNA or a scrambled control for 7 days (Fig. S4D-F). We identified 1,408 differentially expressed genes between conditions (FDR<1%; Fig. 4I, Table 6). KEGG terms such as Alzheimer's, Huntington's, and Parkinson's disease were upregulated upon ARID1A KD in 8GW Fib-iNs, whereas KEGG terms for various types of metabolism and phosphatidylinositol signaling were downregulated upon ARID1A KD (Fig. 4J). Excitingly, when we compared transcriptomic changes to previously published rodent studies as in Fig. 3B-C, we found that ARID1A KD shifted the 8GW Fib-iN transcriptome to increase the expression of genes upregulated in cortical and callosal rodent

neurons during development, and genes downregulated in rodent PNS regenerating neurons (Fig. 4K-L). Further, when we compared DEGs from ARID1A KD in 8GW Fib-iNs to transcripts upregulated in long-growing and short-growing Fib-iNs, we found that ARID1A KD shifted the 8GW transcriptome to be similar to short-growing Fib-iNs, with significant overlap between genes upregulated upon KD and short-growing biased genes, and between genes downregulated upon KD and long-growing biased genes (Fig. 4M-N). Despite *ARID1A* mRNA levels being only ~2 fold with the KD (Fig. S4F), this limited change resulted in a reduced neurite growth phenotype mirrored by a shift of the transcriptomic landscape towards that of short-growing Fib-iNs.

Taken together, here we provide an age-maintained and species-specific model for studying neurite outgrowth and identify an *in vitro* developmental switch in human intrinsic neurite growth ability. We find that direct reprogramming can be used to maintain prenatal age in the resulting neurons. We present a novel transcriptional dataset for human neurons with increased or decreased neurite growth abilities. Finally, we identify ARID1A, a DNA-binding subunit of the cBAF nucleosome remodeling complex, as a developmentally-regulated target which can be modified to enhance human neurite outgrowth.

In the embryonic mouse, *Arid1a* deletion in cortical progenitor cells led to corpus callosum agenesis and mistargeting of intracortical axons (71), whereas *Arid1a* deletion in the neural progenitors of subplate neurons, the first neurons made in the cortex which pioneer the first axon tracts (72), led to decreased growth of descending subplate pioneer axons and loss of subsequent co-fasciculation (71). In the adult mouse, *Arid1a* deletion in retinal ganglion cells prior to optic nerve crush had no effect on regeneration (73). Indeed, our findings in human Fib-iNs would suggest the opposite strategy in the adult CNS, using *Arid1a* overexpression to increase regeneration. In excitatory human neurons derived from embryonic stem cells, *ARID1A* knockout results in decreased dendritic length and reduced synaptic markers (74), though only dendritic growth specifically was measured. Taken together, these and other studies have established a role for ARID1A in pioneer axon growth, dendritic complexity, and synaptic density.

Importantly, identification of ARID1A as a neurite growth regulator implicates chromatin modifiers as important for neurite growth and the lifelong reduction in CNS regenerative abilities, as previously suggested by other studies (75-79). However, what drives these chromatin

5 modifications during development is yet unknown. As we find that environmentally naïve human neurons that have never seen another brain region or brain cell demonstrate a loss of intrinsic neurite growth ability similar to what has been seen in rodent CNS neurons, this suggests that an intrinsic clock may drive these changes. Whether these changes are initiated in the body through systemic signals during specific stages of development or the passage of time itself is yet to be determined.

References

1. J. Bickenbach, A. Officer, T. Shakespeare, P. v. Groote. (2013).
2. A. Tedeschi, F. Bradke, Spatial and temporal arrangement of neuronal intrinsic and extrinsic mechanisms controlling axon regeneration. *Current opinion in neurobiology* **42**, 118-127 (2017).
3. D. L. Moore *et al.*, KLF family members regulate intrinsic axon regeneration ability. *Science* **326**, 298-301 (2009).
4. J. L. Goldberg, M. P. Klassen, Y. Hua, B. A. Barres, Amacrine-signaled loss of intrinsic axon growth ability by retinal ganglion cells. *Science* **296**, 1860-1864 (2002).
5. I. Dusart, M. S. Airaksinen, C. Sotelo, Purkinje cell survival and axonal regeneration are age dependent: an in vitro study. *The Journal of neuroscience : the official journal of the Society for Neuroscience* **17**, 3710-3726 (1997).
6. D. F. Chen, S. Jhaveri, G. E. Schneider, Intrinsic changes in developing retinal neurons result in regenerative failure of their axons. *Proceedings of the National Academy of Sciences of the United States of America* **92**, 7287-7291 (1995).
7. M. Blackmore, P. C. Letourneau, Changes within maturing neurons limit axonal regeneration in the developing spinal cord. *Journal of neurobiology* **66**, 348-360 (2006).
8. E. F. Trakhtenberg *et al.*, Zinc chelation and Klf9 knockdown cooperatively promote axon regeneration after optic nerve injury. *Experimental neurology* **300**, 22-29 (2018).
9. J. Galvao *et al.*, The Kruppel-Like Factor Gene Target Dusp14 Regulates Axon Growth and Regeneration. *Investigative ophthalmology & visual science* **59**, 2736-2747 (2018).
10. M. G. Blackmore *et al.*, Kruppel-like Factor 7 engineered for transcriptional activation promotes axon regeneration in the adult corticospinal tract. *Proceedings of the National Academy of Sciences of the United States of America* **109**, 7517-7522 (2012).
11. M. G. Blackmore *et al.*, High content screening of cortical neurons identifies novel regulators of axon growth. *Molecular and cellular neurosciences* **44**, 43-54 (2010).
12. A. Apará *et al.*, KLF9 and JNK3 Interact to Suppress Axon Regeneration in the Adult CNS. *The Journal of neuroscience : the official journal of the Society for Neuroscience* **37**, 9632-9644 (2017).
13. W. Pita-Thomas, T. M. Goncalves, A. Kumar, G. Zhao, V. Cavalli, Genome-wide chromatin accessibility analyses provide a map for enhancing optic nerve regeneration. *Scientific reports* **11**, 14924 (2021).
14. J. Mertens *et al.*, Directly Reprogrammed Human Neurons Retain Aging-Associated Transcriptomic Signatures and Reveal Age-Related Nucleocytoplasmic Defects. *Cell stem cell* **17**, 705-718 (2015).
15. J. Mertens *et al.*, Age-dependent instability of mature neuronal fate in induced neurons from Alzheimer's patients. *Cell stem cell* **28**, 1533-1548 e1536 (2021).
16. Y. Tang, M. L. Liu, T. Zang, C. L. Zhang, Direct Reprogramming Rather than iPSC-Based Reprogramming Maintains Aging Hallmarks in Human Motor Neurons. *Front Mol Neurosci* **10**, 359 (2017).
17. C. J. Huh *et al.*, Maintenance of age in human neurons generated by microRNA-based neuronal conversion of fibroblasts. *eLife* **5**, (2016).
18. M. B. Victor *et al.*, Striatal neurons directly converted from Huntington's disease patient fibroblasts recapitulate age-associated disease phenotypes. *Nature neuroscience* **21**, 341-352 (2018).

19. Y. M. Oh *et al.*, Age-related Huntington's disease progression modeled in directly reprogrammed patient-derived striatal neurons highlights impaired autophagy. *Nature neuroscience* **25**, 1420-1433 (2022).
20. Y. Kim *et al.*, Mitochondrial Aging Defects Emerge in Directly Reprogrammed Human Neurons due to Their Metabolic Profile. *Cell reports* **23**, 2550-2558 (2018).
21. B. Tasic *et al.*, Shared and distinct transcriptomic cell types across neocortical areas. *Nature* **563**, 72-78 (2018).
22. R. D. Hodge *et al.*, Conserved cell types with divergent features in human versus mouse cortex. *Nature* **573**, 61-68 (2019).
23. B. Chen, L. R. Schaevitz, S. K. McConnell, Fezl regulates the differentiation and axon targeting of layer 5 subcortical projection neurons in cerebral cortex. *Proceedings of the National Academy of Sciences of the United States of America* **102**, 17184-17189 (2005).
24. J. G. Chen, M. R. Rasin, K. Y. Kwan, N. Sestan, Zfp312 is required for subcortical axonal projections and dendritic morphology of deep-layer pyramidal neurons of the cerebral cortex. *Proceedings of the National Academy of Sciences of the United States of America* **102**, 17792-17797 (2005).
25. B. J. Molyneaux, P. Arlotta, T. Hirata, M. Hibi, J. D. Macklis, Fezl is required for the birth and specification of corticospinal motor neurons. *Neuron* **47**, 817-831 (2005).
26. J. Mertens, M. C. Marchetto, C. Bardy, F. H. Gage, Evaluating cell reprogramming, differentiation and conversion technologies in neuroscience. *Nature reviews. Neuroscience* **17**, 424-437 (2016).
27. L. Zhou-Yang *et al.*, Direct Conversion of Human Fibroblasts to Induced Neurons. *Methods Mol Biol* **2352**, 73-96 (2021).
28. T. A. Bedrosian *et al.*, Lamin B1 decline underlies age-related loss of adult hippocampal neurogenesis. *The EMBO journal* **40**, e105819 (2021).
29. M. K. Bin Imtiaz *et al.*, Declining lamin B1 expression mediates age-dependent decreases of hippocampal stem cell activity. *Cell stem cell* **28**, 967-977 e968 (2021).
30. A. Freund, R. M. Laberge, M. Demaria, J. Campisi, Lamin B1 loss is a senescence-associated biomarker. *Molecular biology of the cell* **23**, 2066-2075 (2012).
31. I. Matias *et al.*, Loss of lamin-B1 and defective nuclear morphology are hallmarks of astrocyte senescence in vitro and in the aging human hippocampus. *Aging cell* **21**, e13521 (2022).
32. M. Li *et al.*, Integrative functional genomic analysis of human brain development and neuropsychiatric risks. *Science* **362**, (2018).
33. D. M. Werling *et al.*, Whole-Genome and RNA Sequencing Reveal Variation and Transcriptomic Coordination in the Developing Human Prefrontal Cortex. *Cell reports* **31**, 107489 (2020).
34. M. Pletikos *et al.*, Temporal specification and bilaterality of human neocortical topographic gene expression. *Neuron* **81**, 321-332 (2014).
35. V. Gorbunova *et al.*, The role of retrotransposable elements in ageing and age-associated diseases. *Nature* **596**, 43-53 (2021).
36. K. K. Park *et al.*, Promoting axon regeneration in the adult CNS by modulation of the PTEN/mTOR pathway. *Science* **322**, 963-966 (2008).
37. A. Tedeschi *et al.*, The Calcium Channel Subunit Alpha2delta2 Suppresses Axon Regeneration in the Adult CNS. *Neuron* **92**, 419-434 (2016).
38. A. D. Workman, C. J. Charvet, B. Clancy, R. B. Darlington, B. L. Finlay, Modeling transformations of neurodevelopmental sequences across mammalian species. *The*

- Journal of neuroscience : the official journal of the Society for Neuroscience* **33**, 7368-7383 (2013).
39. B. J. Hilton, F. Bradke, Can injured adult CNS axons regenerate by recapitulating development? *Development* **144**, 3417-3429 (2017).
- 5 40. C. Kiyoshi, A. Tedeschi, Axon growth and synaptic function: A balancing act for axonal regeneration and neuronal circuit formation in CNS trauma and disease. *Developmental neurobiology* **80**, 277-301 (2020).
41. S. Horvath, DNA methylation age of human tissues and cell types. *Genome biology* **14**, R115 (2013).
- 10 42. J. T. Wang *et al.*, Disease gene candidates revealed by expression profiling of retinal ganglion cell development. *The Journal of neuroscience : the official journal of the Society for Neuroscience* **27**, 8593-8603 (2007).
43. P. Arlotta *et al.*, Neuronal subtype-specific genes that control corticospinal motor neuron development in vivo. *Neuron* **45**, 207-221 (2005).
- 15 44. M. Curcio, F. Bradke, Axon Regeneration in the Central Nervous System: Facing the Challenges from the Inside. *Annual review of cell and developmental biology* **34**, 495-521 (2018).
45. M. W. Norisworthy *et al.*, Sox11 Expression Promotes Regeneration of Some Retinal Ganglion Cell Types but Kills Others. *Neuron* **94**, 1112-1120 e1114 (2017).
- 20 46. G. H. D. Poplawski *et al.*, Injured adult neurons regress to an embryonic transcriptional growth state. *Nature* **581**, 77-82 (2020).
47. Y. Sekine *et al.*, Functional Genome-wide Screen Identifies Pathways Restricting Central Nervous System Axonal Regeneration. *Cell reports* **23**, 415-428 (2018).
48. R. P. Smith *et al.*, Transcriptional profiling of intrinsic PNS factors in the postnatal mouse. *Molecular and cellular neurosciences* **46**, 32-44 (2011).
- 25 49. F. Sun *et al.*, Sustained axon regeneration induced by co-deletion of PTEN and SOCS3. *Nature* **480**, 372-375 (2011).
50. P. Langfelder, S. Horvath, WGCNA: an R package for weighted correlation network analysis. *BMC bioinformatics* **9**, 559 (2008).
- 30 51. P. Langfelder, S. Horvath, Fast R Functions for Robust Correlations and Hierarchical Clustering. *J Stat Softw* **46**, (2012).
52. Y. Zhou *et al.*, Metascape provides a biologist-oriented resource for the analysis of systems-level datasets. *Nature communications* **10**, 1523 (2019).
53. D. C. Berwick, G. R. Heaton, S. Azeggagh, K. Harvey, LRRK2 Biology from structure to dysfunction: research progresses, but the themes remain the same. *Mol Neurodegener* **14**, 49 (2019).
- 35 54. L. Civiero, S. Cogo, A. Biosa, E. Greggio, The role of LRRK2 in cytoskeletal dynamics. *Biochemical Society transactions* **46**, 1653-1663 (2018).
55. F. Dajas-Bailador *et al.*, microRNA-9 regulates axon extension and branching by targeting Map1b in mouse cortical neurons. *Nature neuroscience* **15**, 697-699 (2012).
- 40 56. S. A. Giusti *et al.*, MicroRNA-9 controls dendritic development by targeting REST. *eLife* **3**, (2014).
57. J. Jiang *et al.*, MicroRNA-9 regulates mammalian axon regeneration in peripheral nerve injury. *Mol Pain* **13**, 1744806917711612 (2017).
- 45 58. A. Alfert, N. Moreno, K. Kerl, The BAF complex in development and disease. *Epigenetics Chromatin* **12**, 19 (2019).

59. T. Kosho, N. Okamoto, C. Coffin-Siris Syndrome International, Genotype-phenotype correlation of Coffin-Siris syndrome caused by mutations in SMARCB1, SMARCA4, SMARCE1, and ARID1A. *Am J Med Genet C Semin Med Genet* **166C**, 262-275 (2014).
60. S. Xu, C. Tang, The Role of ARID1A in Tumors: Tumor Initiation or Tumor
5 Suppression? *Front Oncol* **11**, 745187 (2021).
61. S. Blumli *et al.*, Acute depletion of the ARID1A subunit of SWI/SNF complexes reveals distinct pathways for activation and repression of transcription. *Cell reports* **37**, 109943 (2021).
62. J. R. Raab, S. Resnick, T. Magnuson, Genome-Wide Transcriptional Regulation
10 Mediated by Biochemically Distinct SWI/SNF Complexes. *PLoS genetics* **11**, e1005748 (2015).
63. M. Trizzino *et al.*, The Tumor Suppressor ARID1A Controls Global Transcription via Pausing of RNA Polymerase II. *Cell reports* **23**, 3933-3945 (2018).
64. R. Mathur *et al.*, ARID1A loss impairs enhancer-mediated gene regulation and drives
15 colon cancer in mice. *Nature genetics* **49**, 296-302 (2017).
65. B. H. Alver *et al.*, The SWI/SNF chromatin remodelling complex is required for maintenance of lineage specific enhancers. *Nature communications* **8**, 14648 (2017).
66. M. R. Wilson *et al.*, ARID1A Mutations Promote P300-Dependent Endometrial Invasion through Super-Enhancer Hyperacetylation. *Cell reports* **33**, 108366 (2020).
- 20 67. F. De Virgiliis *et al.*, Enriched conditioning expands the regenerative ability of sensory neurons after spinal cord injury via neuronal intrinsic redox signaling. *Nature communications* **11**, 6425 (2020).
68. T. H. Hutson *et al.*, Cbp-dependent histone acetylation mediates axon regeneration induced by environmental enrichment in rodent spinal cord injury models. *Sci Transl Med* **11**, (2019).
- 25 69. I. Palmisano *et al.*, Epigenomic signatures underpin the axonal regenerative ability of dorsal root ganglia sensory neurons. *Nature neuroscience* **22**, 1913-1924 (2019).
70. H. C. Hodges *et al.*, Dominant-negative SMARCA4 mutants alter the accessibility landscape of tissue-unrestricted enhancers. *Nat Struct Mol Biol* **25**, 61-72 (2018).
- 30 71. D. Z. Doyle *et al.*, Chromatin remodeler Arid1a regulates subplate neuron identity and wiring of cortical connectivity. *Proceedings of the National Academy of Sciences of the United States of America* **118**, (2021).
72. S. K. McConnell, A. Ghosh, C. J. Shatz, Subplate neurons pioneer the first axon pathway from the cerebral cortex. *Science* **245**, 978-982 (1989).
- 35 73. X. Q. Peng *et al.*, Loss of Arid1a Promotes Neuronal Survival Following Optic Nerve Injury. *Frontiers in cellular neuroscience* **14**, 131 (2020).
74. P. P. Liu *et al.*, Acetate supplementation restores cognitive deficits caused by ARID1A haploinsufficiency in excitatory neurons. *EMBO molecular medicine* **14**, e15795 (2022).
75. I. Venkatesh, V. Mehra, Z. Wang, B. Califf, M. G. Blackmore, Developmental chromatin
40 restriction of pro-growth gene networks acts as an epigenetic barrier to axon regeneration in cortical neurons. *Developmental neurobiology*, (2018).
76. F. Muller *et al.*, CBP/p300 activation promotes axon growth, sprouting, and synaptic plasticity in chronic experimental spinal cord injury with severe disability. *PLoS biology* **20**, e3001310 (2022).
- 45 77. Y. Lu *et al.*, Reprogramming to recover youthful epigenetic information and restore vision. *Nature* **588**, 124-129 (2020).

78. P. Gaub *et al.*, HDAC inhibition promotes neuronal outgrowth and counteracts growth cone collapse through CBP/p300 and P/CAF-dependent p53 acetylation. *Cell death and differentiation* **17**, 1392-1408 (2010).
79. P. Gaub *et al.*, The histone acetyltransferase p300 promotes intrinsic axonal regeneration. *Brain : a journal of neurology* **134**, 2134-2148 (2011).

Acknowledgments:

General: We thank Jake Kirkland and Jeffrey Goldberg for comments on the manuscript; the UW-Madison Flow Cytometry core (P30 CA014520 and 1S10RR025483-01); We thank The Birth Defects Research Laboratory for human brain tissue, supported by NIH award number 5R24HD000836 from the Eunice Kennedy Shriver National Institute of Child Health and Human Development; D. Gamm and A. Bhattacharyya for patient fibroblast samples and iPSC lines; J. Mertens for assistance with the direct reprogramming protocol; and members of the Moore lab and UW-Madison community for their input. Artwork was created on Biorender.

Funding:

Hilldale-Holstrom Fellowship (to EANT)

National Institutes of Health grant 1R21NS111192 (to DLM)

National Institutes of Health grant F30NS122478-01 (to BPL)

National Institutes of Health grant T32GM140935 (to UW-Madison Medical Scientist Training Program, BPL)

National Institutes of Health grant T32AG052374 (to RJL and BBT)

National Institutes of Health grant R35GM142395 (to BAB)

Author contributions:

Conceptualization: BPL, EANT, DLM

Investigation: BPL, EANT, KR, ZPA, PCK, ERP, RR, AMMS, RJL

Analysis: BPL, EANT, KR, BAB

Methodology: EANT, DLM

Software: SS, DW, BAB, BBT, CSM

Funding acquisition: DLM, BAB

Resources: AB

Supervision: BPL, DLM

Visualization: BPL, EANT, DLM

Writing – original draft: BPL, DLM

Writing – review & editing: BPL, EANT, DLM, AMMS, AB, BAB

Competing interests: Authors declare that they have no competing interests.

Data and materials availability: Processed data are found in the tables. Raw RNA sequencing datafiles found at dbGaP (phs003285.v1.p1)

5

http://www.ncbi.nlm.nih.gov/projects/gap/cgi-bin/study.cgi?study_id=phs003285.v1.p1

Supplementary Materials

Materials and Methods

10

Figs. S1-S4

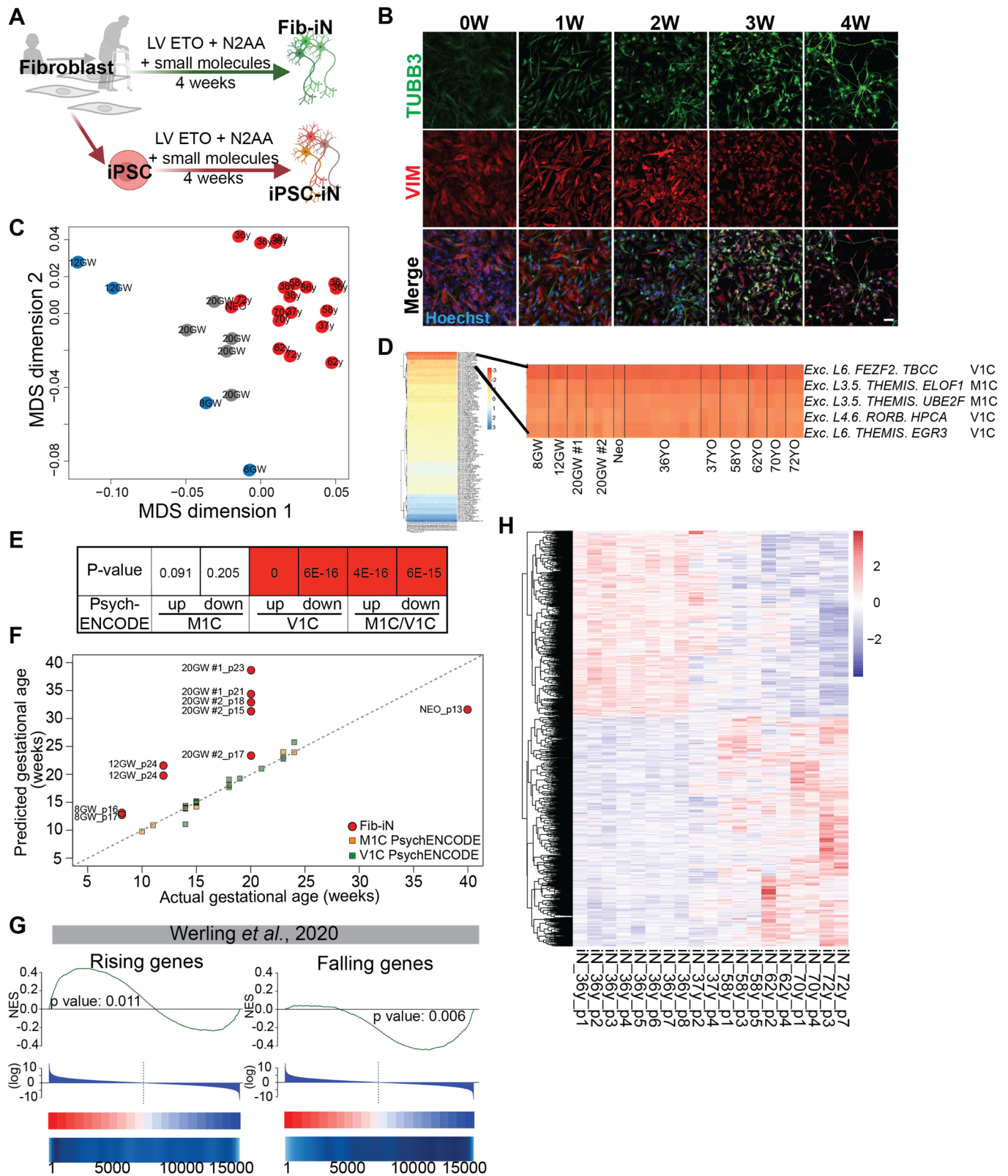


Figure 1: Fib-iNs transdifferentiated from fetal through adult human fibroblasts preserve age.

A-B) 8GW to 72YO human fibroblasts were reprogrammed to Fib-iNs by overexpressing

NEUROG2 and ASCL1 (N2AA) in a doxycycline-dependent manner (LV ETO), followed by 4 weeks of transdifferentiation in induction media. As an age-reset control, 5 of the original fibroblast ages were reprogrammed to iPSCs, then transdifferentiated using the same overexpression paradigm to generate iPSC-iNs. **B)** 36YO fibroblasts were immunostained over the 4 weeks of transdifferentiation to Fib-iNs for beta-III tubulin (TUBB3; neurons), vimentin (VIM; fibroblasts), and Hoechst (nuclei). Scale bar = 100 μ m. **C)** Multi-dimensional scaling (MDS) of RNA-seq data for all Fib-iN samples. **D)** Spearman rank correlation (Rho) of Fib-iN RNA-seq to neuronal expression profiles from the Allen Brain Map single cell human data of various brain regions (21, 22), revealing that all ages of Fib-iNs are most similar to excitatory neurons (Exc.) of primary motor cortex (M1C) and primary visual cortex (V1C). **E)** Comparison of Fib-iN DEGs enriched in long-growing (8GW-12GW) vs. short-growing (NEO-72YO) against genes up and downregulated in human “M1C only”, “V1C only”, and “M1C and V1C” cortical development from PsychENCODE (32) with associated p-values. FDR <0.001 (V1C and V1C/M1C), FDR<0.013 (M1C UP), FDR<0.22 (M1C DOWN). **F)** Using machine-learning, RNA-seq from PsychENCODE’s human developmental M1C and V1C brain regions was used to train a model to predict the age of Fib-iN samples from RNA-seq profiles (32), revealing increasing developmental age from gestational age Fib-iNs, irrespective of passage number (p). **G)** Heatmap of significant age-related transcriptional changes in adult Fib-iNs (36YO-72YO; 2,431 genes) with an FDR<5%. **H)** Gene set enrichment analysis using genesets from human dorsolateral prefrontal cortex samples (33) showing genes rising during development (left) and genes falling in development (right) are enriched in short-growing (positive values) and long-growing Fib-iNs (negative values), respectively.

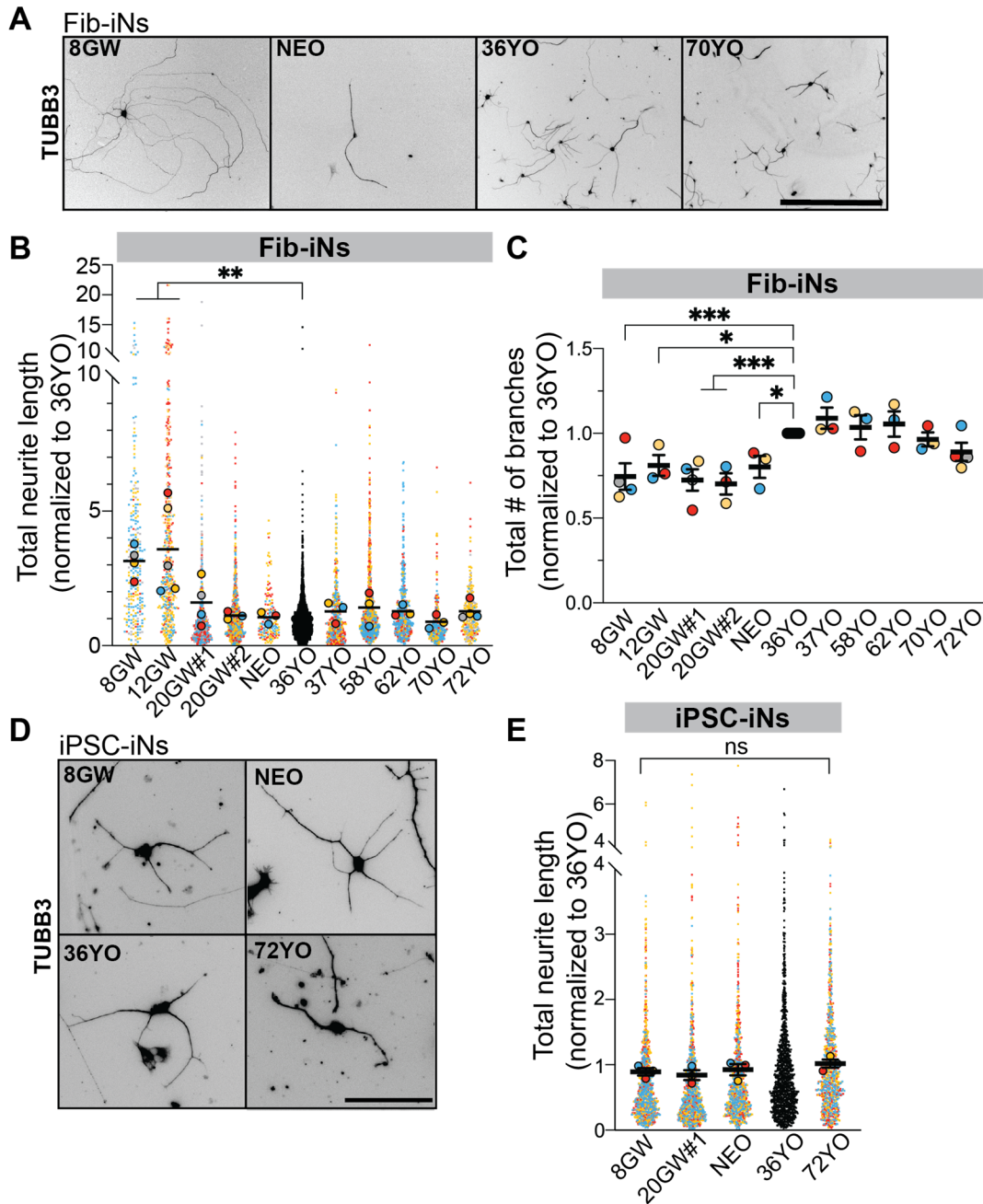


Figure 2: Conservation of a developmental loss of intrinsic neurite outgrowth in human neurons.

A-B) Fib-iNs of all ages were trypsinized, and plated for 2 days in ASM before fixation, and immunostaining for TUBB3. Neurons were imaged and traced for total neurite length. A superplot shows total neurite length of all Fib-iN ages normalized to their within-batch 36YO sample. One-way ANOVA with post-hoc Tukey's test on averages of replicates compared to 36YO; Mean \pm SEM. **C)** The number of total branches per neuron were averaged from each age, and normalized to the 36YO sample of each experiment. One-way ANOVA with post-hoc Tukey's test on averages

of replicates compared to 36YO; Mean \pm SEM. **D-E**) iPSC-iNs were trypsinized, and plated for 2 days in ASM before fixation, and immunostaining for TUBB3. A superplot shows total neurite length of all iPSC-iN ages normalized to their within-batch 36YO sample. One-way ANOVA with post-hoc Tukey's test on averages of replicates; Mean \pm SEM. For all experiments, $N \geq 3$ different inductions, $n \geq 50$ cells per induction. Scale bar (A) 500 μm , (E) 100 μm . ns = not significant, * $p < 0.05$ ** $p < 0.01$ *** $p < 0.001$.

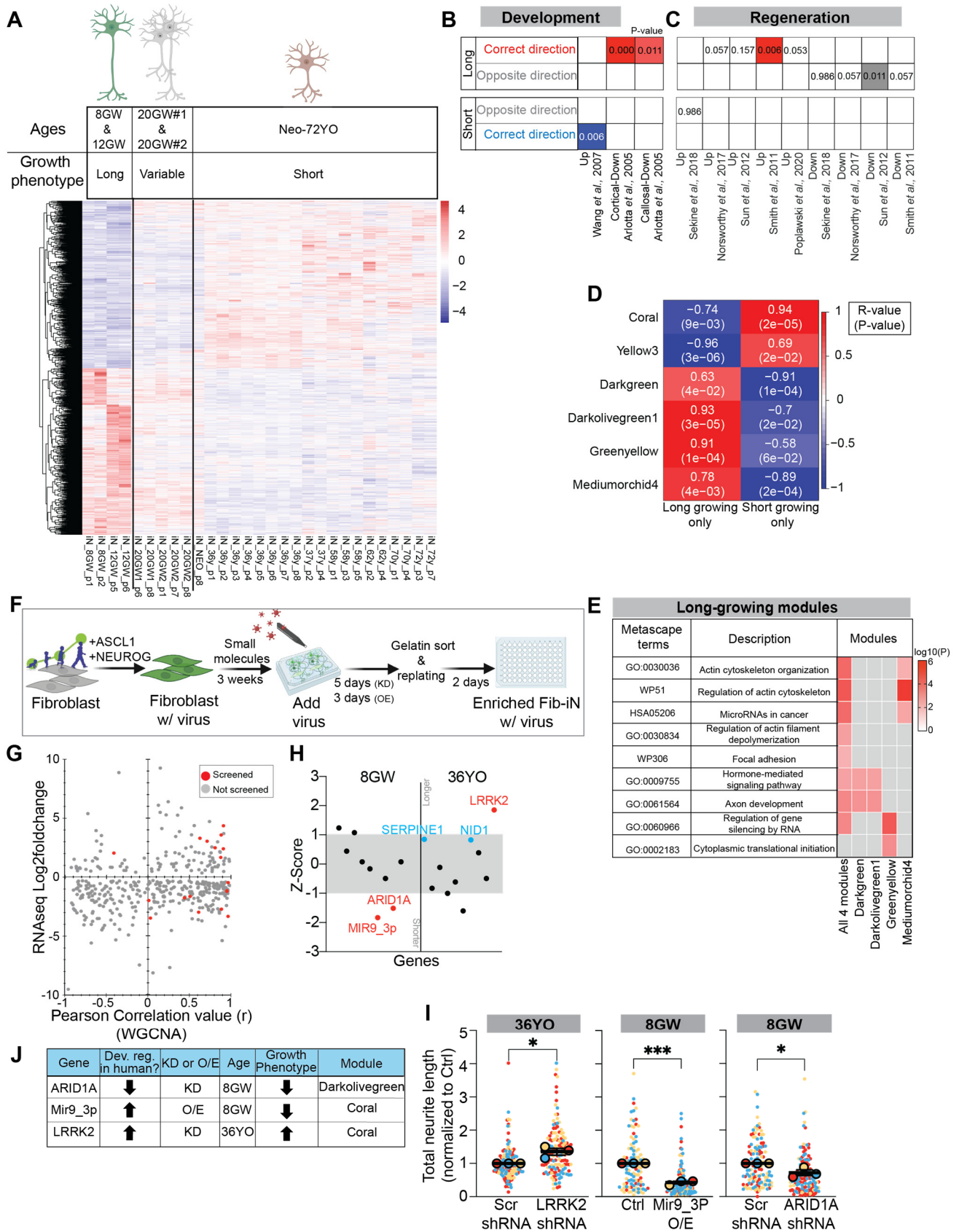


Figure 3: Developmentally-regulated genes screened in Fib-iNs reveal multiple drivers of

human neurite growth.

A) RNA-seq of 11 ages of Fib-iNs revealed 3,465 differentially expressed genes (DEGs) with FDR <1%. Schematic of RNA-seq analysis strategy, with “long-growing” (8GW & 12GW) vs. “short-growing” (Neo to 72YO). 20GW #1 and #2 are only provided for a visual comparison and were not included in the differential analysis due to having “variable” growth. **B)** Gene Set Enrichment Analysis (GSEA) for curated genes from developmentally-regulated rodent datasets (orthologs) in long- and short-growing Fib-iNs. Long= genes upregulated in long-growing iNs; short= genes upregulated in short-growing iNs; Up= genes upregulated in rodent developmental datasets, down= genes downregulated in rodent developmental datasets. FDR <0.05 and consistent (red or blue boxes), FDR >0.05 (white boxes), FDR <0.05 but inconsistent (grey boxes). **C)** GSEA for curated gene lists from regenerative rodent datasets (orthologs) in long and short growing Fib-iNs. Up= genes upregulated in regeneration, down= genes downregulated in regeneration. FDR are as in B. **D)** Pearson correlation values and p-values of 6 most significant eigengenes and traits from WGCNA analysis. **E)** Significant Metascape term enrichment in long-growing modules. **F)** Schematic of screen paradigm for overexpression or knockdown of specific genes in Fib-iNs. **G)** Pearson correlation value (r) of genes from the 6 key modules plotted against their respective RNA-seq log2foldchange. Positive r value indicates positively correlated with short-growing phenotype, negative r value indicates positively correlation with long-growing phenotype. Positive log2foldchange indicates gene enrichment in short-growing Fib-iN ages. Negative log2foldchange indicates gene enrichment in long-growing Fib-iN ages. Red dots = genes screened, grey dots = genes not screened. **H)** Z-score of genes tested in 36YO and 8GW Fib-iNs in primary screen. Shaded grey area is 1 standard deviation in each direction. Both red and blue dotted genes were tested in secondary screen, with only red dots successfully reproducing primary screen results. **I)** Secondary screen of 5 primary screen hits, showing the significant genes’ total neurite length normalized to its appropriate control (ctrl; plasmid overexpression (GFP O/E) or scrambled (Scr) shRNA (shRNA)). N ≥ 3 different inductions, n ≥ 50 cells per induction. Student T-test. Mean ± SEM. **J)** Table summary showing secondary screen gene hits, expression trend in human cortex during development (PsychENCODE), knockdown (KD) or overexpression (O/E), age of Fib-iN tested, resulting growth phenotype in the tested Fib-iN age, and WGCNA module. ns = not significant *p<0.05, ***p<0.001.

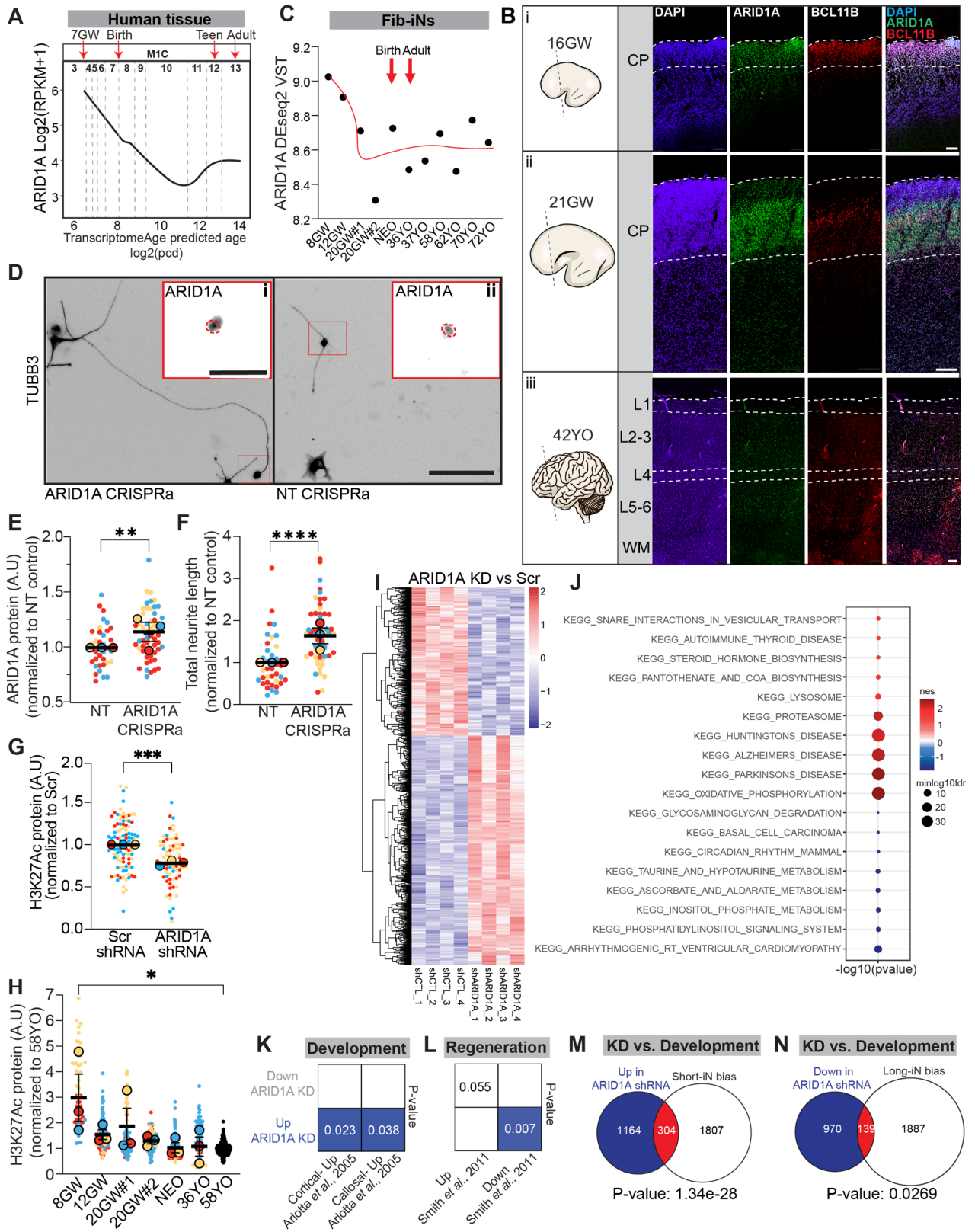


Figure 4: ARID1A is a developmentally-regulated driver of human neurite growth.

A) ARID1A transcript levels (Log₂(RPKM+1)) across development in human M1C

(PsychENCODE). Post conception day (PCD). Time is displayed in epochs. **B**) Immunostaining of ARID1A in 16GW (i), 21GW (ii) and 42YO (iii) human prefrontal cortex shows colocalization of ARID1A and deep layer neurons (BCL11B). Layer (L) 1-6, CP= cortical plate, WM= white matter. Scale bar, 200 μ m. **C**) Average ARID1A transcript expression (DEseq2 VST) across all Fib-iN ages. **D**) Representative images of *ARID1A* CRISPRa (left) and NT (right) control in 36YO Fib-iN, stained for neuronal identity (TUBB3), and ARID1A protein. Scale bar, 100 μ m (D), 50 μ m (Di, ii). Red circle = nuclei. **E-F**) Quantification of ARID1A protein levels (**E**) with CRISPRa for 7 days in 36YO Fib-iN, and neurite length (**F**; normalized to NT control). Student t-test on averages of replicates; Mean \pm SEM. N \geq 3 different inductions, n=20 cells per induction. **G-H**) Superplot quantification of immunostained H3K27acetylation (H3K27Ac) protein levels **G**) 7-days post ARID1A or Scr shRNA transduction in 8GW Fib-iNs (normalized to Scr shRNA of each experiment), and **H**) across development (normalized to the 58YO of each experiment). N=3 different inductions, n=30 cells per induction. **I**) 1,408 DEGs (FDR <1%) were identified in RNA-seq of ARID1A shRNA vs. Scr shRNA 7 days post-transduction in 8GW Fib-iNs. **J**) Top KEGG pathways significantly enriched in ARID1A shRNA KD as compared to Scr ctrl (red: upregulated with KD, blue: downregulated with KD). **K-L**) Comparison of transcripts upregulated and downregulated in ARID1A KD 8GW Fib-iNs against the same (**K**) developmental and (**L**) regeneration rodent datasets from Fig. 3C-D reveals a similarity of genes upregulated in ARID1A KD and upregulated with development. Up= genes upregulated in rodent datasets; down= genes downregulated in rodent datasets. FDR of <0.05. **M**) Venn diagram revealing the overlap of genes upregulated with ARID1A KD in 8GW Fib-iNs to genes upregulated in short-growing Fib-iNs (Neo-72YO). Fisher's exact test. **N**) Genes downregulated with ARID1A KD in 8GW Fib-iNs had greater overlap with genes upregulated in long-growing Fib-iNs (8-12GW). Fisher's exact test. Arbitrary units (A.U.). *p<0.05 **p<0.01 ***p<0.001 ****p<0.0001

25

Tables:

Table 1: Original fibroblasts used for experiments.

Table 2: Fib-iN RNA-seq DEG VSTs across all the ages and experimental replicates.

Table 3: WGCNA analysis of all the genes from Fib-iN RNA-seq and their eigengenes.

5 Table 4: All the genes within the 6 selected eigengenes.

Table 5: Details on genes tested in Fib-iN gene screen.

Table 6: ARID1A shRNA knockdown vs. scrambled control shRNA DEGs.